Received: 29 August 2016 | Revised: 19 November 2017 | Accepted: 21 November 2017

DOI: 10.1111/mec.14452

ORIGINAL ARTICLE

WILEY MOLECULAR ECOLOGY

# Evidence for miRNA-mediated modulation of the host transcriptome in cnidarian–dinoflagellate symbiosis

Sebastian Baumgarten[1] | Maha J. Cziesielski[1] | Ludivine Thomas[2] | Craig T. Michell[1] | Lisl Y. Esherick[3] | John R. Pringle[3] | Manuel Aranda[1] | Christian R. Voolstra[1]

[1]Division of Biological and Environmental Science and Engineering, Red Sea Research Center, King Abdullah University of Science and Technology, Thuwal, Saudi Arabia

[2]Bioscience Core Laboratory, King Abdullah University of Science and Technology, Thuwal, Saudi Arabia

[3]Department of Genetics, Stanford University School of Medicine, Stanford, CA, USA

**Correspondence**
Christian R. Voolstra, Red Sea Research Center, King Abdullah University of Science and Technology (KAUST), Thuwal, Saudi Arabia.
Email: christian.voolstra@kaust.edu.sa
and
John R. Pringle, Department of Genetics, Stanford University School of Medicine, Stanford, CA, USA.
Email: jpringle@stanford.edu

**Present addresses**
Sebastian Baumgarten, Biology of Host-Parasite Interactions Unit, Institut Pasteur, Paris, France.
Ludivine Thomas, HM.Clause, Portes-lès-Valence, France.
Lisl Y. Esherick, Department of Biological Engineering, Massachusetts Institute of Technology, Cambridge, MA, USA.

**Funding information**
King Abdullah University of Science and Technology; Gordon and Betty Moore Foundation, Grant/Award Number: 2629.01

## Abstract

Reef-building corals and other cnidarians living in symbiotic relationships with intracellular, photosynthetic dinoflagellates in the genus *Symbiodinium* undergo transcriptomic changes during infection with the algae and maintenance of the endosymbiont population. However, the precise regulatory mechanisms modulating the host transcriptome are unknown. Here, we report apparent post-transcriptional gene regulation by miRNAs in the sea anemone *Aiptasia*, a model system for cnidarian–dinoflagellate endosymbiosis. *Aiptasia* encodes mainly species-specific miRNAs, and there appears to have been recent differentiation within the *Aiptasia* genome of miRNAs that are commonly conserved among anthozoan cnidarians. Analysis of miRNA expression showed that both conserved and species-specific miRNAs are differentially expressed in response to endosymbiont infection. Using cross-linking immunoprecipitation of Argonaute, the central protein of the miRNA-induced silencing complex, we identified miRNA binding sites on a transcriptome-wide scale and found that the targets of the miRNAs regulated in response to symbiosis include genes previously implicated in biological processes related to *Symbiodinium* infection. Our study shows that cnidarian miRNAs recognize their mRNA targets via high-complementarity target binding and suggests that miRNA-mediated modulations of genes and pathways are important during the onset and maintenance of cnidarian–dinoflagellate endosymbiosis.

**KEYWORDS**
*Aiptasia*, anemone, Argonaute, coral, cross-linking immunoprecipitation

## 1 | INTRODUCTION

The trophic and structural basis of one of the most important marine ecosystems, coral reefs, relies on a functional endosymbiosis between cnidarian coral hosts and photosynthetic dinoflagellate symbionts in the genus *Symbiodinium*, which reside within vesicles (symbiosomes) in the host's gastrodermal cells (Davy, Allemand, & Weis, 2012). In this mutualistic relationship, the host offers a sheltered environment to the alga and provides the inorganic nutrients needed for photosynthesis and growth, whereas the symbiont transfers the majority of its photosynthetic products to the host (Muscatine & Porter, 1977). This tight nutrient coupling allows the animal–alga pair to grow in extremely oligotrophic waters. Most symbiotic cnidarians acquire their endosymbionts with high specificity from the environment ("horizontally") (Dubinsky & Stambler, 2010), either during the larval phase after sexual reproduction or during the recovery from a stress-induced symbiosis breakdown ("bleaching"). There is growing evidence that the establishment and maintenance of the endosymbiosis are accompanied by specific changes in host gene expression, including genes involved in pattern recognition and innate immunity, endocytosis and transmembrane nutrient transport (Baumgarten et al., 2015; Ganot et al., 2011; Lehnert et al., 2014; Rodriguez-Lanetty, Phillips, & Weis, 2006; Schnitzler & Weis, 2010; Voolstra et al., 2009). However, little is yet known about the higher level regulatory mechanisms that might participate in the modulation and orchestration of such changes in gene expression.

MicroRNAs (miRNAs) are small (~22 nt) noncoding RNAs that post-transcriptionally downregulate gene expression through complementary binding of their target mRNAs. In this process, the mature miRNA first binds to the Argonaute (Ago) protein and guides the miRNA-induced silencing complex (miRISC) to partially complementary target sequences within mRNAs, resulting in translational inhibition or target degradation (Carthew & Sontheimer, 2009). Even though the general mechanism of RNA interference and miRNA action is evolutionarily conserved throughout large parts of the phylogenetic tree, several aspects of miRNA biogenesis and mode of action are distinct, in particular between animals and plants (Shabalina & Koonin, 2008). For instance, plant miRNAs bind their mRNA targets mostly with high complementarity within the coding sequence (CDS), leading to target cleavage. In contrast, most metazoan miRNAs only require short complementarity of 2–8 nt in the miRNA 5′ region (i.e., the "seed") for target recognition in the 3′ UTR that commonly leads to translational repression (Shabalina & Koonin, 2008). Interestingly, dissection of miRNA function in the "basal" metazoan *Nematostella vectensis* showed that although miRNA expression led to translational repression (Mauri et al., 2017), the miRNAs also seem to bind their mRNA targets with high, plant-like complementarity leading to mRNA cleavage (Moran et al., 2014).

One miRNA can have a multitude of mRNA targets and widespread downstream effects, making miRNAs regulatory hubs for the fine-tuning of gene expression and the orchestration of broad transcriptomic changes (Esau et al., 2006). Recent studies have suggested that miRNAs are involved in the interactions of hosts with eukaryotic endoparasites such as *Leishmania donovani* and *Plasmodium falciparum* (Ghosh, Bose, Roy, & Bhattacharyya, 2013; LaMonte et al., 2012), suggesting that miRNA expression and regulation of target genes might also be involved in transcriptome modulation in the cnidarian–dinoflagellate endosymbiotic relationship.

Using the small sea anemone *Aiptasia* as a model system for cnidarian–dinoflagellate symbiosis, we took advantage of its recently sequenced genome (Baumgarten et al., 2015) to investigate the potential role of host miRNA regulation by integrating small RNA and mRNA sequencing at different stages of endosymbiont infection. By establishing a protocol for high-throughput sequencing–cross-linking immunoprecipitation (HITS-CLIP) of the *Aiptasia* Ago protein, we identified high-confidence ternary interactions involving the Ago effector protein, the potentially regulatory miRNAs, and their target mRNA transcripts on a transcriptome-wide scale. Data produced following this approach supported the conclusion that cnidarian miRNAs recognize their mRNA targets via high-complementarity target binding and revealed possible miRNA-mediated modulations of genes and pathways important for a functional symbiosis.

## 2 | MATERIALS AND METHODS

### 2.1 | *Aiptasia* culture

Anemones of the clonal *Aiptasia* strain CC7 (Sunagawa et al., 2009) were used for all experiments and were cultured as described previously (Baumgarten et al., 2015). Briefly, anemones were kept in autoclaved sea water (ASW) at 25°C on a 12-hr:12-hr light–dark cycle (20–40 μmol photons $m^{-2}$ $s^{-1}$ during light cycle) and fed once a week with freshly hatched *Artemia* (brine shrimp) nauplii larvae. Water changes were performed on the days following feedings. Aposymbiotic (dinoflagellate-free) anemones were generated as described previously (Baumgarten et al., 2015) using a combination of cold shocks in the dark at 4°C, treatment with the photosynthesis inhibitor diuron (DCMU) in the light at 25°C, and incubation for ≥6 months in the dark at 25°C with feeding and water changes as before. Prior to experimental use, aposymbiotic *Aiptasia* were acclimatized to a 12-hr:12-hr light–dark cycle for at least two weeks at 25°C and checked by fluorescence stereomicroscopy to verify that they were still devoid of dinoflagellates (as judged by the absence of chlorophyll autofluorescence).

### 2.2 | Infection with *Symbiodinium* and RNA sequencing

To analyse RNA from anemones at different stages of infection, aposymbiotic anemones were infected with the clonal, axenic *Symbiodinium minutum* strain SSB01 (Baumgarten et al., 2015; Xiang, Hambleton, DeNofrio, Pringle, & Grossman, 2013) essentially as described previously (Baumgarten et al., 2015). Briefly, anemones of 5–10 mm oral-disc diameter were held in 6-well plates (Falcon # 353046); each well contained 3–5 anemones and 15 ml of autoclaved and sterile-filtered sea water (ASFW). After 16 d of acclimatization (see above),

infection proceeded as follows: day 1, addition of *Symbiodinium* cells (from a culture growing exponentially in F/2-Si medium; Baumgarten et al., 2013) to a final concentration of ~$10^5$ cells/ml; day 2, feeding (as above) without change of ASFW or adding additional algae; day 3, change of ASFW and addition of algae at ~$10^5$ cells/ml; day 11, end of incubation with *Symbiodinium* cells by moving the anemones into ASFW without algae in fresh 6-well plates; and days 11–30, regular feeding and ASFW changes as above. Samples were taken for RNA analysis at days 1 (before addition of algae; aposymbiotic anemones), 12 (partially populated anemones), and 30 (by which time the anemones should be fully populated) (Hambleton, Guse, & Pringle, 2014). At each time point, the anemones from the six wells of one plate were pooled to form one biological replicate, and four such biological replicates were collected.

Total RNA was extracted using TRIzol (Thermo Fisher # 15596-026), and small RNAs were fractionated using the mirVana small-RNA-enrichment kit (Thermo Fisher # AM1560) following the manufacturer's instructions. All small RNA sequencing libraries were prepared using the Illumina TruSeq Small RNA Sample Library Kit (Illumina # RS-200-0012) and sequenced as single-end reads on one lane of an Illumina HiSeq 2000. The resulting reads are deposited at the NCBI Sequence Read Archive (SRA) (Accession nos.: aposymbiotic, SRX1351928; partially populated, SRX1351929; fully populated, SRX1351930; see Table S1). The processing of mRNA samples and the analysis of differentially expressed genes from the infection experiment were described by (Baumgarten et al., 2015); the mRNA sequences can be accessed at the NCBI SRA (Accession nos.: aposymbiotic, SRX757525; partially populated, SRX757526; symbiotic, SRX757528). To estimate the progression of *Symbiodinium* infection over the 30-day time-course, the mRNA sequences were mapped to a *S. minutum* reference transcriptome (NCBI BioProject Accession no. PRJNA274852) using bowtie2 (Langmead & Salzberg, 2012). The percentages of read pairs that aligned to the symbiont transcriptome without mismatches are shown in Figure S1a.

## 2.3 | miRNA annotation

The small RNA reads were first trimmed by removing adapter sequences and filtered to remove low-quality reads using Trimmomatic (Bolger, Lohse, & Usadel, 2014). Only reads of 15–32 nucleotides were retained, and redundant sequences were collapsed using the collapse_reads.pl script from the miRDeep2 package (Friedlander, Mackowiak, Li, Chen, & Rajewsky, 2012). Next, we annotated the regions of the *Aiptasia* genome encoding noncoding RNAs (ncRNAs), including snoRNAs, snRNAs, tRNAs and rRNAs using reference ncRNA sequences retrieved from the RNAcentral database (The RNAcentral Consortium, 2015) and aligned to the *Aiptasia* genome using BLASTN (*E*-value cut-off ≤1e-5) (Altschul, Gish, Miller, Myers, & Lipman, 1990). The *Aiptasia* ncRNA regions identified by this alignment were then used as a database for mapping of the small RNA reads using bowtie2 (Langmead & Salzberg, 2012). Small RNA reads that mapped to the ncRNA database using bowtie2 were removed before further analyses.

miRNAs were then annotated using the miRDeep2 package with default settings (Friedlander et al., 2012). To identify putatively conserved miRNAs based on previous de novo annotations of other cnidarian genomes, we created a reference library of mature miRNA sequences from *N. vectensis* (Grimson et al., 2008; Moran et al., 2014), *Hydra magnipapillata* (Krishna et al., 2013) and *Stylophora pistillata* (Liew et al., 2014). An initial set of 145 miRNAs was predicted and further inspected for characteristics of *bona fide* miRNAs. These included (i) potential folding of the precursor miRNA transcript (pre-miRNA) into an unbranched hairpin structure, (ii) 5′ ends of small RNA reads mapping uniformly to the pre-miRNA hairpin, (iii) differing frequencies of mature miRNA and star miRNA (i.e., the complementary strand that is not bound to the Ago protein) reads mapping to the pre-miRNA stem and (iv) 2-nt overhangs of the mature miRNA and the star miRNA sequence in the miRNA duplex (sensu Baumgarten et al., 2013; Tarver, Donoghue, & Peterson, 2012). Applying these additional stringent criteria, we identified 46 miRNAs mapping to 60 genomic loci (Table S2). We then used the built-in scoring mechanism of miRDeep2 to assign probabilities of the 46 miRNA to be true positives, performing 100 rounds of permutation (Friedlander et al., 2008, 2012). All 46 miRNAs had true-positive probabilities of detection ≥84%, except for the evolutionarily conserved apa-mir-9454. Reviewing the prediction for apa-mir-9454 showed that no star sequences for this miRNA were recovered in the *Aiptasia* small RNA libraries, decreasing its probability of identification by the algorithm. However, because of the perfect conservation of the mature miRNA sequence, we retained apa-mir-9454 for subsequent analyses.

## 2.4 | miRNA differential expression and motif analysis

To assess expression levels of miRNAs, we mapped each set of preprocessed small RNA reads (i.e., small RNAs retained after ncRNA filtering) independently to the identified miRNA precursor sequences using the script quantifier.pl from the miRDeep2 package (Friedlander et al., 2012). The miRNA read counts of each replicate were then normalized to the total number of mapped small RNA reads to allow for comparison between samples. These analyses were performed with three replicates for each time point of the infection experiment (see above) using the EDGER package (Robinson, McCarthy, & Smyth, 2010) implemented in R (R Development Core Team, 2012). The *Z*-scores of miRNAs showing significant differential expression (FDR ≤ 0.01) were then calculated over all replicates/infection states and visualized in MeV (Howe, Sinha, Schlauch, & Quackenbush, 2011). Briefly, *Z*-scores over all samples/replicates (i.e., "rows") were calculated following the formula $Z = (x - u)/s$, with $x$ = actual miRNA count; $u$ = average miRNA count over all samples, and $s$ = miRNA standard deviation over all samples. Multidimensional scaling (MDS) plots were created in EDGER using the "plotMDS" function. Distances between pairs of RNA samples correspond to the average root mean squares of the largest absolute log2 fold-changes (R Development Core Team, 2012; Robinson et al., 2010).

To identify motifs putatively involved in the transcriptional control of the one apa-mir-2022a and two apa-mir-2022b loci (see Section 3), we extracted the 1 kb of sequence upstream of the pre-miRNA start position of each locus. The motif analysis was performed using the MEME web suite (Bailey et al., 2009), searching for up to 10 motifs that occur zero or only one time per region. For comparison, the 1 kb of sequence downstream of each locus was also used for motif identification using the same settings.

## 2.5 | Generation and testing of anti-AipAgo1 antibody

*Aiptasia* Argonaute (AipAgo) proteins were identified by BLASTP alignments of the *N. vectensis* Ago protein sequences (UniProt Accession nos. U3MIG1, U3MH35) to the *Aiptasia* genomic protein set (http://aiptasia.reefgenomics.org) (*E*-value ≤1e-5). From the canonical AipAgo1, a peptide of 25 amino acids (residues 811–835) (Figure S1b) was selected to be used as antigen. To ensure that it was specific to AipAgo1, the peptide sequence was searched against the entire *Aiptasia* genomic protein set (Baumgarten et al., 2015) using BLASTP (*E*-value cut-off ≤1e-5) (Altschul et al., 1990); no significant alignment was found other than the corresponding position in AipAgo1 itself. This peptide was subsequently synthesized and used for the generation of polyclonal antibodies (Acris Antibodies, Herford, Germany). Briefly, antibodies (Ab) were raised in rabbits following immunization with 1 mg of KLH (keyhole limpet haemocyanin)-conjugated peptide antigen. The antigen-specific Ab titre was determined with an enzyme-linked immunosorbent assay (ELISA) using horseradish peroxidase (HRP) conjugated to anti-rabbit-IgG Ab and ATBS (2,2′-azinobis [3-ethylbenzothiazoline-6-sulfonic acid]-diammonium salt) as substrate. Abs were affinity-purified from the serum of the highest titre bleed using the synthesized peptide antigen on a cyanogen bromide-activated agarose column.

To test the specificity of the antibodies by Western blotting, *Aiptasia* lysates were prepared by sampling ~15 adult anemones (5–10 mm oral-disc diameter) in ice-cold PBS and grinding them into pieces of several $mm^3$ with a plastic mortar and pestle. Following centrifugation (200*g*, 10 min, 4°C), the tissue pellet was resuspended in three volumes of NP-40 cell lysis buffer (Thermo Fisher # FNN0021) supplemented with 1 mM PMSF and a protease-inhibitor cocktail (Sigma-Aldrich # P2714) according to the manufacturers' instructions. The tissue samples were then disrupted using a Wheaton glass homogenizer, incubated on ice for 30 min and centrifuged (16,000*g*, 10 min, 4°C); the protein-containing supernatant was then sampled for further processing. Proteins were resolved electrophoretically on a 12% SDS–polyacrylamide gel for ~1.5 hr at 120 V using a 2-gel Tetra and Blotting Module (Bio-Rad # 1660828EDU) and transferred to a PVDF membrane for 2 hr at 100 V using the same module. After blocking overnight at 4°C using StartingBlock T20 (PBS) (Thermo Fisher # 37538), the membrane was incubated for 2 hr at 37°C with 20 μg of Ab diluted 1:1,000 in Tris-buffered saline (pH = 7.5) supplemented with 0.05% (v/v) Tween-20 (TBST), followed by 3-hr incubation at room temperature with a goat-anti-rabbit-IgG secondary Ab tagged with DyLight Fluor 488 (Thermo Fisher # A-11034) diluted 1:10,000 in TBST. Each incubation with antibodies was followed by extensive washes with TBST to remove any nonspecific binding. Protein bands were visualized using a Typhoon Scanner 9410 (GE Healthcare).

## 2.6 | Immunohistochemical staining

For whole-mount staining, anemones were placed in a six-well plate with ASFW, stunned for 15 min with 0.2% magnesium chloride and then incubated in 1% formaldehyde for 20 min at room temperature. The fixed anemones were transferred to 1.5-ml microcentrifuge tubes and washed in 500 μl PBST (phosphate-buffered saline with 0.1% Triton X-100) for 15 min on a spin-wheel at room temperature. For antigen exposure, the PBST was removed, and the anemones were suspended in 500 μl of 10 nM sodium citrate in sterile water and incubated in a water bath at 99°C for 30 min. Subsequently, the anemones were washed with PBST and incubated for 2 hr in PBSTB blocking solution at room temperature. For staining, the samples were incubated in anti-AipAgo1 primary antibody (dilution: 1:250 in PBSTB) or in PBSTB alone (negative control) overnight at 4°C on a spin-wheel. The samples were washed twice with PBSTB for 10 min per wash, followed by incubation with Dylight Fluor 650-tagged goat-anti-rabbit-IgG secondary antibody (Thermo Fisher #84546) for 2 hr at room temperature. DNA staining followed the protocol described below.

Aposymbiotic anemones were macerated according to (David, 1973). Briefly, whole animals were placed in a maceration solution containing glycerine, glacial acetic acid and water (ratio 1:1:13) at room temperature. The tissue was left soaking for 30 min with

**FIGURE 1** Overview of the AipAgo1 cross-linking immunoprecipitation (CLIP) experiment and sequence analysis. (a) Workflow for the CLIP experiments (see Section 2). The tripartite miRNA–mRNA–Ago complex was cross-linked with UV light in vivo followed by cell lysis and immunoprecipitation of AipAgo1 and the bound RNA. After digestion of mRNA with RNase A/T1 (preserving only tags protected by AipAgo1 around the miRNA binding site), the protein–RNA complexes were resolved by molecular size using SDS-gel electrophoresis and blotted to a nitrocellulose membrane. The region corresponding to the molecular weight of AipAgo1 (~96 kDa) was excised (Panel c), protein was digested with proteinase K, and RNA was extracted and prepared for sequencing (Panel e). TSAP, thermosensitive alkaline phosphatase; T4 PNK, T4 polynucleotide kinase. (b) Red line, electropherogram showing length distribution of RNA tags extracted immediately after step 3 (Panel a; see Section 2). Blue line, same with a control IgG; no RNA tags were detected after immunoprecipitation and RNase digestion. (c) Western blot of AipAgo1-RNA complexes. The red box indicates the membrane area that was excised for further processing. (d) Like (b), but showing the length distribution of RNA tags that were extracted from the nitrocellulose membrane after the complete CLIP procedure (Panel a, step 5). (e) Workflow for analysis of the CLIP-tags (see Section 2 for details) [Colour figure can be viewed at wileyonlinelibrary.com]

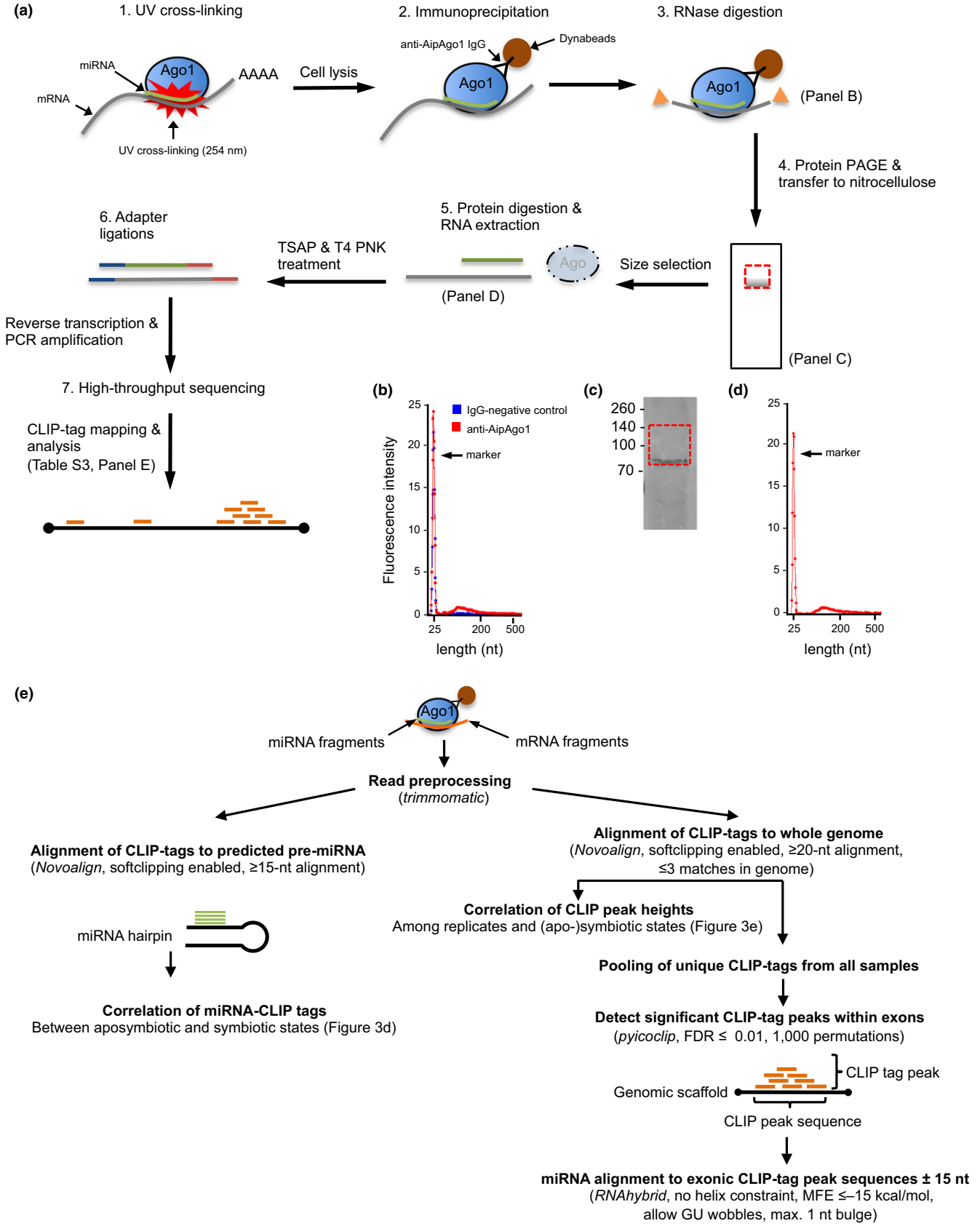


occasional gentle shaking until the animals were visibly dissociated. The resulting cell suspension was fixed by addition of 0.1 volume of 20% (v/v) formaldehyde and incubated for 15 min at room temperature. About 50–100 μl of the fixed cell suspension was subsequently spread on superfrost microscope slides, allowed to dry at room temperature and incubated twice for 15 min with PBST. Slides

were then incubated for 2 hr in PBSTB blocking solution (PBST containing 1% [w/v] bovine serum albumin and 10% [w/v] goat serum [Southern Biotech # 0060-01]). For staining, slides were incubated either with the purified anti-AipAgo1 Ab (dilution: 1:250 in PBSTB) or in PBSTB alone (negative control) in a humidified chamber at 4°C overnight. Next, Dylight Fluor 650-tagged goat-anti-rabbit-IgG secondary antibody (Thermo Fisher # 84546) was added after 1:400 dilution in PBSTB, and the slides were incubated for 1 hr in a humidified chamber at room temperature. Cells were subsequently stained also for actin using Dylight 488 Phalloidin (Thermo Fisher # 21833) and DNA using Hoechst 33342 (Thermo Fisher # H1399) for 30 and 15 min, respectively. Between every staining incubation step, slides were washed three times for 15 min each in PBST.

## 2.7 | Cross-linking immunoprecipitation and RNA sequencing

For these experiments (see overview in Figure 1a), we used aposymbiotic and fully populated anemones, with two replicates for each symbiotic state. For each replicate, ~15 adult anemones (5–10 mm oral-disc diameter) were transferred into ice-cold PBS and ground on ice into pieces of several $mm^3$ with plastic mortar and pestle without further addition of grinding agents. The samples were then placed in 10-cm Petri dishes in ~8 ml of ice-cold PBS on ice and irradiated three times at 254 nm with 400 mJ/$cm^2$ (actual energy received by the sample; ~3 min for each irradiation) using a Spectrolinker XL-1000 UV cross-linker (Spectronics). Samples were swirled for ~30 s in the Petri dishes between each irradiation to cool and maximize surface UV exposure for cross-linking. Preparation of cell lysates using NP-40 lysis buffer was then performed as described above. Final protein concentrations of the cross-linked cell lysates (~3 μg/μl) were measured by Bradford assay (Bio-Rad # 5000202).

To immunoprecipitate the cross-linked RNA -AipAgo1 complexes from the lysates, 20 μg of the affinity-purified anti-AipAgo1 Ab was bound to 100 μl of Protein G-coated Dynabeads (Thermo Fisher #100007D) for each sample according to the manufacturer's protocol and then incubated with 700 μl of lysate for 1 hr at 4°C with end-over-end rotation. The beads were then washed twice with 400 μl of washing buffer (provided with the Dynabeads kit) per wash at room temperature. The mRNA bound to AipAgo1 complexes was trimmed on the beads for 6 min at room temperature using 0.4 U RNase A/T1 (Thermo Fisher # EN0551) diluted in 400 μl washing buffer, followed immediately by one additional wash of the beads using 400 μl washing buffer to remove residual RNase A/T1. The RNA -AipAgo1 complexes were then eluted from the Dynabeads using 60 μl elution buffer consisting of 39 μl of the elution buffer provided with the kit supplemented with 15 μl 4× NuPAGE LDS (lithium dodecyl sulphate) sample buffer (Thermo Fisher # NP0008) and 6 μl 10× NuPAGE reducing agent (Thermo Fisher # NP0004). Beads diluted in the premixed elution solution were heated for 10 min at 70°C, and the supernatant was collected for SDS-PAGE analysis (see below).

As an initial positive control for successful RNA co-immunoprecipitation, RNAs were isolated directly from the Dynabeads (after RNase digestion and washing) using TRIzol LS (Thermo Fisher # 10296010) and the mirVana small-RNA-enrichment kit (Thermo Fisher # AM1560) and visualized on a Bioanalyzer 2100 (Agilent Technologies, RNA Pico Chip) (Figure 1b). As a negative control, a mock immunoprecipitation was performed using a nonspecific goat anti-mouse-IgG Ab (Thermo Fisher # 35502), and RNAs that might have copurified with the antibody were again isolated directly from the beads and analysed as just described (Figure 1b).

To remove copurified contaminants that had survived the immunoprecipitation and washes, the RNase-digested immunoprecipitate was subjected to SDS-PAGE. A 20-μl aliquot was loaded into each lane of a Novex NuPAGE Bis-Tris 4%–12% mini gel (Thermo Fisher # NP0321BOX), and the proteins were resolved by electrophoresis for 1 hr at 150 V using NuPAGE MOPS running buffer (Thermo Fisher # NP0001) in a X-Cell SureLock Mini-Cell (Thermo Fisher # EI0002). To further ensure the removal of any free RNA that had comigrated with the RNA -AipAgo1 complexes, proteins were then transferred for 2 hr at 100 V to a nitrocellulose membrane (Sigma-Aldrich # GE10600002) using 10% (v/v) methanol NuPAGE transfer buffer (Thermo Fisher # NP0006) in a 2-gel Transfer and Blotting Module (Bio-Rad # 1660828EDU).

RNAs were then isolated from the regions of the nitrocellulose membranes that should contain the AipAgo1 protein (predicted molecular weight ~96 kDa) and larger RNA -AipAgo1 complexes (Figure 1c). The membrane regions were excised, cut into 1- to 2-mm squares and collected in RNase-free microcentrifuge tubes. Proteins were then digested by mixing the cut membrane pieces with 400 μl 1× TE buffer containing 0.5% (w/v) SDS and 150 μg proteinase K (Qiagen # 19131), incubating for 2 hr at 55°C in a thermoblock, and shaking at 1,000 rpm. RNA was isolated from the supernatants using TRIzol LS and the mirVana kit following the manufacturers' instructions and then visualized using the Bioanalyzer 2100; this step also allowed assessment of the expected trimming of the protein-bound RNA to a length of ~50–100 nt during the earlier RNase treatment (Figure 1d).

To sequence the miRNA and mRNA fragments, they were first dephosphorylated using thermosensitive alkaline phosphatase (NEB # M0371) and then treated with T4 polynucleotide kinase to specifically phosphorylate their 5′ ends as preparation for RNA sequencing adapter ligation. Sequencing libraries were then prepared using the TruSeq small-RNA-library prep kit (Illumina # RS-200-0012) following the manufacturer's instructions, with 24 cycles of final library PCR amplification. The resulting cDNA libraries were sequenced single-end (1 × 101 bp) on one lane of an Illumina HiSeq 2000. The sequences are deposited at the NCBI SRA (Accession no. SRX1351926).

## 2.8 | HITS-CLIP sequence analyses

As outlined in Figure 1e, sequences obtained from the HITS-CLIP experiment were first trimmed of adapter sequences and filtered

to remove low-quality sequences using Trimmomatic (Bolger et al., 2014). For the detection of miRNAs, reads were then aligned to the pre-miRNA sequences obtained from the miRNA annotation (miRDeep2) using NovoAlign (http://www.novocraft.com), requiring a minimum alignment of 15 nucleotides and allowing soft clipping of the read ends (Figure 1e, left). The numbers of reads mapping to each pre-miRNA were then tested for correlation between the replicates for each biological sample after first normalizing the raw counts for each sample by the total number of CLIP sequences that aligned to pre-miRNAs in the respective library (Figure 1e, right).

For analysis of the immunoprecipitated RNA fragments (i.e., CLIP-tags), the reads were aligned to the whole genome using NovoAlign, requiring a minimum alignment of 20 nucleotides, allowing a read to match no more than three times in the genome, and enabling soft clipping of the read ends (Figure 1e, right). Subsequent filtering and analysis were performed following the scripts and pipeline described by Moore et al. (2014) (http://zhanglab.c2b2.columbia.edu/index.php/CIMS). Briefly, the sequence alignments were first converted into the BED file format for convenient handling of all subsequent analysis steps, and putative PCR duplicates were then collapsed based on the alignment coordinates (i.e., reads having the exact same start and end alignment position were counted only once) to create a set of unique CLIP-tags in each of the four samples (Table S3). Overlapping CLIP-tags (i.e., CLIP-tag peaks) and their respective heights (i.e., numbers of CLIP-tags per peak) were then identified, requiring a minimum overlap of one nucleotide within a peak. The bedtools "intersect" tool (Quinlan, 2014) was used to identify genomic regions that showed CLIP-tag peaks across all samples. The CLIP-tag heights were normalized as for the CLIP miRNA counts (see above), and the normalized heights of the CLIP-tag peaks containing three or more CLIP-tags at the same genomic region in each sample were tested for correlation.

Pyicoclip (Althammer, Gonzalez-Vallinas, Ballare, Beato, & Eyras, 2011) was used to identify significant CLIP-tag peaks within mRNA exons, using the pooled, unique CLIP-tags from all four samples. Pyicoclip implements the modified FDR algorithm proposed by Yeo et al. (2009) and was run with 1,000 rounds of permutation. Briefly, pyicoclip calculates the background frequency of detected CLIP-tag peaks by randomly placing the same number of CLIP-tags into exonic regions and calculating the probability of obtaining the same CLIP-tag peak height as from the actual data. Only exonic CLIP-tag peaks with a FDR value $\leq$0.01 were retained for further analyses. The numbers of CLIP-tag peaks falling in each type of exonic region (i.e., 5′ UTR, coding sequence, or 3′ UTR) were obtained from the genome-feature file (gff) of the *Aiptasia* genome assembly. The CLIP-tag peak sequences (i.e., the genomic regions covered from the start of the first CLIP-tag within the peak to the end of the last CLIP-tag in the same peak) plus the regions of 15-nucleotide upstream and 15-nucleotide downstream were then extracted from the *Aiptasia* genome using bedtools "getfasta" (Quinlan, 2014). Next, RNAhybrid (Krüger & Rehmsmeier, 2006) was used to map the 46 *bona fide* miRNAs (see above) to the CLIP-tag peak sequences requiring (i) no a priori helix constraints and (ii) a minimum free energy of binding (MFE) $\leq$−15 kcal/mol, while allowing (iii) GU wobbles in the miRNA-target alignment and (iv) a maximum of 1-nt bulges on either side of the alignment. When a CLIP-tag peak region was targeted by multiple miRNAs, we only retained the interaction that showed the highest number of binding nucleotides between the miRNA and the CLIP-tag peak region.

For comparison of miRNA–mRNA complementarity between *Aiptasia* and published mammalian CLIP data sets, we retrieved the human miRNA CLIP data that were initially sampled by Kishore et al. (2011) and reanalysed by Grosswendt et al. (2014) for the presence of chimeric miRNA–mRNA reads to unambiguously identify miRNA–mRNA target sites. We mapped the human miRNA to their respective mRNA target site using RNAhybrid (Krüger & Rehmsmeier, 2006) and calculated the numbers of interacting miRNA nucleotides with the same settings as described above.

## 3 | RESULTS

### 3.1 | Annotation of conserved and species-specific miRNAs in *Aiptasia*

We investigated the *Aiptasia* miRNA repertoire using replicate small RNA libraries prepared from *Aiptasia* polyps at different stages of infection (aposymbiotic, partially populated and fully populated) with the endosymbiotic *S. minutum* strain SSB01 (see Section 2, Figure 2a and Figure S1a, and Table S1). Initial inspection of the small RNA reads revealed a length distribution with an apparent overrepresentation of two small RNA populations with nucleotide lengths of 19–23 and 27–31 nucleotides, respectively (Figure 2b). The former represent putative miRNAs and small-interfering RNAs (siRNAs), whereas the latter represent putative PIWI-interacting RNAs (piRNAs) and constituted the majority of the sequenced small RNAs. Both the length distribution and the strong bias towards uridine in the 5′ position of both small RNA populations (Figure 2b) are consistent with studies of other cnidarians (Grimson et al., 2008; Juliano et al., 2014; Krishna et al., 2013; Liew et al., 2014; Moran et al., 2014).

From the pooled small RNA samples, we annotated 46 high-confidence miRNAs, transcribed from a total of 60 distinct genomic loci (Table S2), after stringent filtering (see Section 2) for known characteristics of metazoan miRNAs that reflect the evolutionary conservation of their biogenesis pathway in animals (Moran et al., 2014). These characteristics include (i) a distinct length of ~21–23 nt; (ii) predicted folding of the pre-miRNA transcript into a hairpin structure of ~60 nt; (iii) homogeneous 5′ ends of the mature miRNA reads resulting from the precise cleavage of the pre-miRNA by the Dicer endonuclease; and (iv) unequal frequencies of small RNA reads mapping to the opposite sides of the pre-miRNA hairpin stem. The last characteristic is attributed to the strand-selection process in which the mature miRNA is bound to the Ago effector protein while the complementary sequence of the stem (star-miRNA) is degraded (Figure 2c). Eleven of the 46 miRNAs were identical in sequence to ones that had been annotated previously in one or more other anthozoan

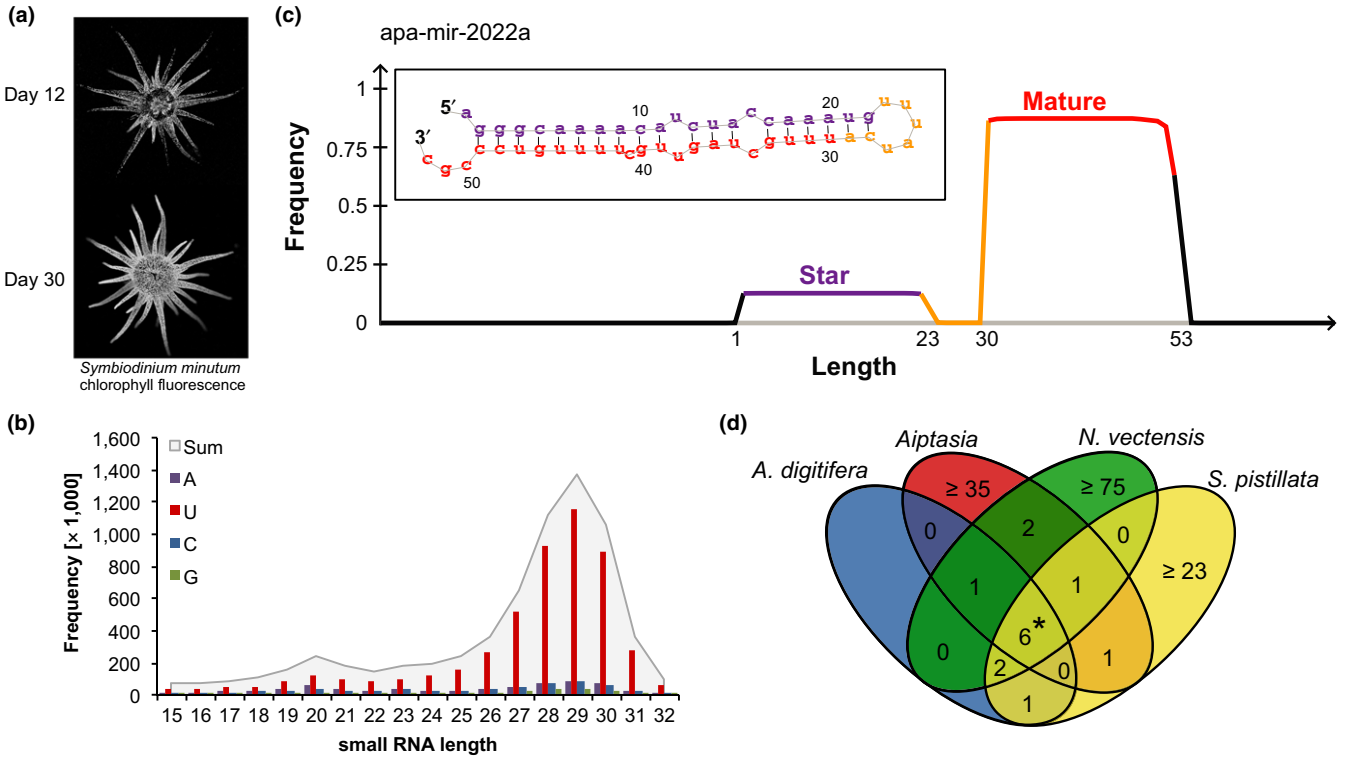


**FIGURE 2** Annotation of the *Aiptasia* miRNA repertoire. (a) Increase of *Symbiodinium* cell numbers after infection of aposymbiotic *Aiptasia*, as visualized by the intensity of the red fluorescence of the algal chlorophyll (shown here in black and white) in partially populated (12 days post infection, top) and fully populated (30 days post infection, bottom) animals. (b) Overrepresentation of two populations of small RNA reads corresponding to putative siRNAs/miRNAs (19–23 nt) and putative piRNAs (27–31 nt). At each length, the small RNA reads are sorted by their 5′ nucleotide (coloured bars), and the sum at each length is shown as the grey area. (c) Example of a miRNA (apa-mir-2022a) matching all criteria for *bona fide* miRNA annotation. Box, predicted secondary hairpin structure of the pre-miRNA as predicted using RNAfold (Hofacker, 2003) within miRDeep2 (Friedlander et al., 2012). Bottom, the relative frequencies of small RNA reads that map to the opposite sides of the hairpin (ordinate) are shown along an axis corresponding to the primary pre-miRNA sequence (abscissa). Reads matching the mature miRNA sequence (red) have homogeneous 5′ ends and considerably higher read counts than do those matching the complementary strand (star-miRNA; purple). Both star and mature miRNA sequence have a distinct length of 23 nt. (d) Overlap of evolutionarily conserved mature miRNAs in the anthozoans for which data are available; the numbers of conserved and distinct species are indicated. Only six miRNAs (denoted by the *) are found in all four species: mir-100, mir-2022, mir-2023, mir-2030, mir-2036 and mir-2050 [Colour figure can be viewed at wileyonlinelibrary.com]

species (Grimson et al., 2008; Juliano et al., 2014; Krishna et al., 2013; Liew et al., 2014; Moran et al., 2014), with only six being conserved among all the anthozoans for which there are data available (Figure 2d). The largest overlap ($n$ = 10) was found with the closest relative of *Aiptasia* among the species studied, the starlet sea anemone *N. vectensis*.

## 3.2 | Identification of mRNA–miRNA–protein interactions in vivo

To confirm the identification of *Aiptasia* miRNAs and identify functional molecular interactions between them and their cognate target mRNAs, we conducted high-throughput sequencing cross-linking immunoprecipitation (HITS-CLIP) experiments using antibodies against *Aiptasia* Ago, the core protein of the miRNA-induced silencing complex. The *Aiptasia* genome encodes two Ago proteins that differ in length like their homologs in *N. vectensis* (Moran, Praher, Fredman, & Technau, 2013). The predicted sequence of the canonical protein (AipAgo1) is 853 amino acids long, like the Ago proteins of mammals, whereas the second protein is predicted to be considerably longer (1,083 aa). We focused on AipAgo1 and raised polyclonal antibodies against a peptide antigen in its C-terminus (see Section 2 and Figure S1b). After affinity purification, the antibodies recognized predominantly a single polypeptide of approximately the expected size (~96 kDa) in Western blots of whole anemone extracts (Figure 3a). Immunofluorescence staining of whole-mount *Aiptasia* polyps indicated that AipAgo1 is present throughout the organism (Figure 3b), as expected. In isolated cells, AipAgo1 appeared to be distributed throughout the cytoplasm but clustered locally at sites that putatively correspond to Processing (P-) bodies (Figure 3c) (Leung & Sharp, 2013).

We then followed an established CLIP protocol for the identification of RNA–protein interactions, including ternary miRNA–mRNA–Ago interactions (Chi, Zang, Mele, & Darnell, 2009; Moore et al., 2014) (see Section 2 and Figure 1a). After UV cross-linking of miRNAs to their target mRNAs and the Ago protein, the free mRNA

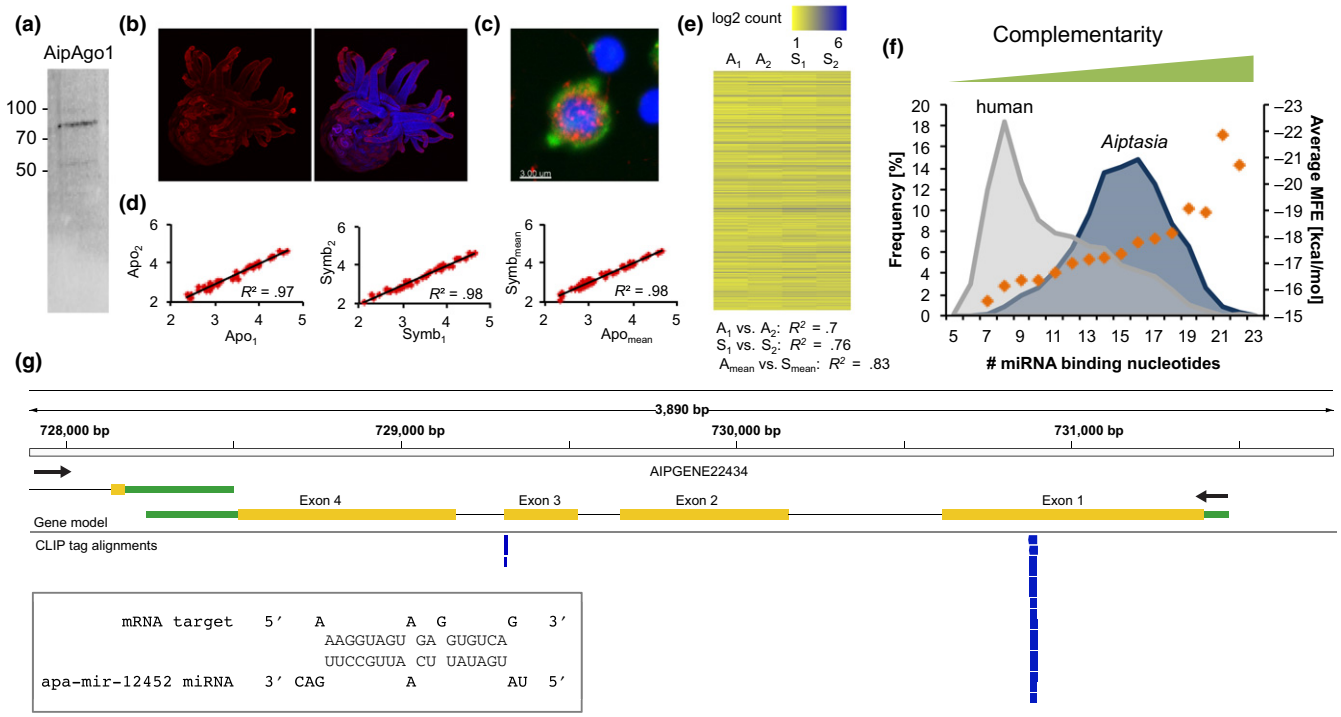


**FIGURE 3** Cross-linking immunoprecipitation (CLIP) of *Aiptasia* Argonaute AipAgo1. (a) Western blot of *Aiptasia* extract showing that the antibody recognizes a polypeptide at the expected size of AipAgo1. (b) Left, whole-mount immunofluorescence staining of AipAgo1 showing the presence of the protein throughout *Aiptasia* polyps. Right, overlay of AipAgo1 immunofluorescence (red) and Hoechst staining of nuclei (blue). (c) Subcellular localization of AipAgo1. Red, immunofluorescence staining of AipAgo1; blue, Hoechst staining of nuclei; green, staining of the actin cytoskeleton with Dylight 488-labelled phalloidin (see Section 2). Note accumulation of AipAgo1 in particular locations that presumably correspond to P-bodies. (d) Correlations between the miRNA read counts (log10 values) from the independent cross-linking immunoprecipitation (CLIP) experiments for the two replicates of aposymbiotic anemones (left), the two replicates of fully populated symbiotic anemones (middle), and the means of the two replicates for each of the two symbiotic states (right). (e) Correlation of the CLIP-tag peak heights across the genome in the two independent replicates of the CLIP experiment with aposymbiotic animals ($A_1$, $A_2$) and the two replicates with symbiotic animals ($S_1$, $S_2$). The rows represent the various genomic regions with ≥3 CLIP-tags in each of the replicates; the columns represent the four replicates. The correlation coefficients are shown below. (f) Frequencies (%) of miRNA–mRNA interactions with various numbers of miRNA nucleotides involved in mRNA target binding (blue area: *Aiptasia* CLIP data [this study]; grey area: Human CLIP data; Grosswendt et al., 2014; Kishore et al., 2011, left-hand axis). The average minimum free energy of binding for each of the miRNA–mRNA interactions in the *Aiptasia* data is shown as orange diamonds (right-hand axis). (g) Genome-browser view of the region containing a gene (systematic name AIPGENE22434) that encodes a cnidarian Ficolin-like protein (CniFL; see Baumgarten et al., 2015). Most CLIP-tags of the pooled aposymbiotic and symbiotic samples mapped to a single narrow region (blue boxes below Exon 1 in the gene model), which putatively represents a target site of apa-mir-12452. A few other CLIP-tags mapped to the 3′ end of Exon 3; the significance of this mapping is unclear. The box at lower left shows the sequence of apa-mir-12452 complementary to the putative mRNA target site. Green, untranslated regions; yellow, coding sequences; narrow lines, introns; arrows, directions of transcription [Colour figure can be viewed at wileyonlinelibrary.com]

tails, both upstream and downstream of the miRNA-Ago-binding sites, are digested with RNase. The protection from nuclease digestion by the Ago protein ensures that only miRNAs and mRNA sequences ("CLIP-tags") corresponding to the Ago-binding site are processed further. The exclusive sequencing of CLIP-tags enables the subsequent detection of Ago-binding sites with high confidence by searching for specific enrichments (i.e., peaks) that mark the sites of putative miRNA–mRNA interactions (Figure 1a,e). We performed CLIP experiments on two biological replicates of aposymbiotic anemones and two replicates of fully populated symbiotic anemones. In a first step, we aligned the immunoprecipitated RNAs to the *bona fide* miRNAs annotated by miRDeep2 and found that all 46 predicted miRNAs corresponded to CLIP-tags (Figure 1e). We also found that the numbers of CLIP-tags mapping to the predicted, annotated pre-miRNAs correlated well both between replicates (Figure 3d, left and middle) and between the two symbiotic states (Figure 3d, right).

We next aligned the CLIP-tags to the *Aiptasia* genome using stringent criteria of processing and filtering (see Section 2; Figure 1e), obtaining totals of 112,903 and 195,897 aligned CLIP-tags from the two aposymbiotic and the two symbiotic samples, respectively (Table S3). Examination of the clusters of overlapping CLIP-tags (≥1-nt overlap) at distinct genomic loci showed that the numbers of CLIP-tags per cluster also correlated well both between the two replicates for each symbiotic state and between the two symbiotic states (Figure 3c).

The high correlation between replicates observed with both the Ago-miRNA (Figure 3d) and Ago-mRNA (Figure 3e) interactions suggests that the CLIP protocol has high technical reproducibility and

robustness, as observed also in previous studies (Chi et al., 2009; Weyn-Vanhentenryck et al., 2014). In addition, the interactions identified in the aposymbiotic and symbiotic samples (Figure 3d,e) revealed only limited differences in the overall numbers of interactions. The fine-tuned regulation of mRNA transcripts levels might therefore originate from quantitative (i.e., differential expression of targeting miRNAs) rather than from qualitative (i.e., different miRNA–mRNA interactions) differences. Thus, although it is possible that infection state-specific differences in miRNA–mRNA–Ago interactions may yet be detected, we pooled the CLIP-tags of all four biological samples for subsequent analyses.

We next associated significant CLIP-tag peaks with exonic regions using the modified false discovery rate (FDR) algorithm proposed by Yeo et al. (2009) and implemented in pyicoclip (Althammer et al., 2011) (see Section 2). This analysis yielded a set of 2,269 CLIP-tag peaks (FDR ≤0.01), with an average length of 60 nt, which represent putative sites of mRNA-Ago binding. The majority (63%) of these peaks lay within the protein-coding sequences of transcripts, with an additional 27% and 10% falling within 5′ and 3′ UTRs, respectively.

To identify functionally significant sites of miRNA–mRNA binding, we next mapped the *bona fide* mature miRNAs annotated by miRDeep2 to the identified CLIP-tag peak sequences (i.e., the genomic sequence from the start to the end of the CLIP-tag peak). This analysis identified 3,377 interactions between a miRNA and an mRNA-Ago site with a minimum free energy of binding of ≤−15 kcal/mol (Table S4). A total of 2,758 of these interactions included a single CLIP-tag peak sequence and a single miRNA, whereas 619 CLIP-tag peak sequences showed more than one equally good mRNA interaction with a miRNA. Further inspection of these 619 interactions showed that 226 CLIP-tag peak sequences were targeted by two almost identical miRNAs, apa-mir-2022a and apa-mir-2022b, and another 30 CLIP-tag peak sequences were targeted by a single miRNA multiple times and equally well (i.e., with the same number of binding miRNA nucleotides; see Section 2).

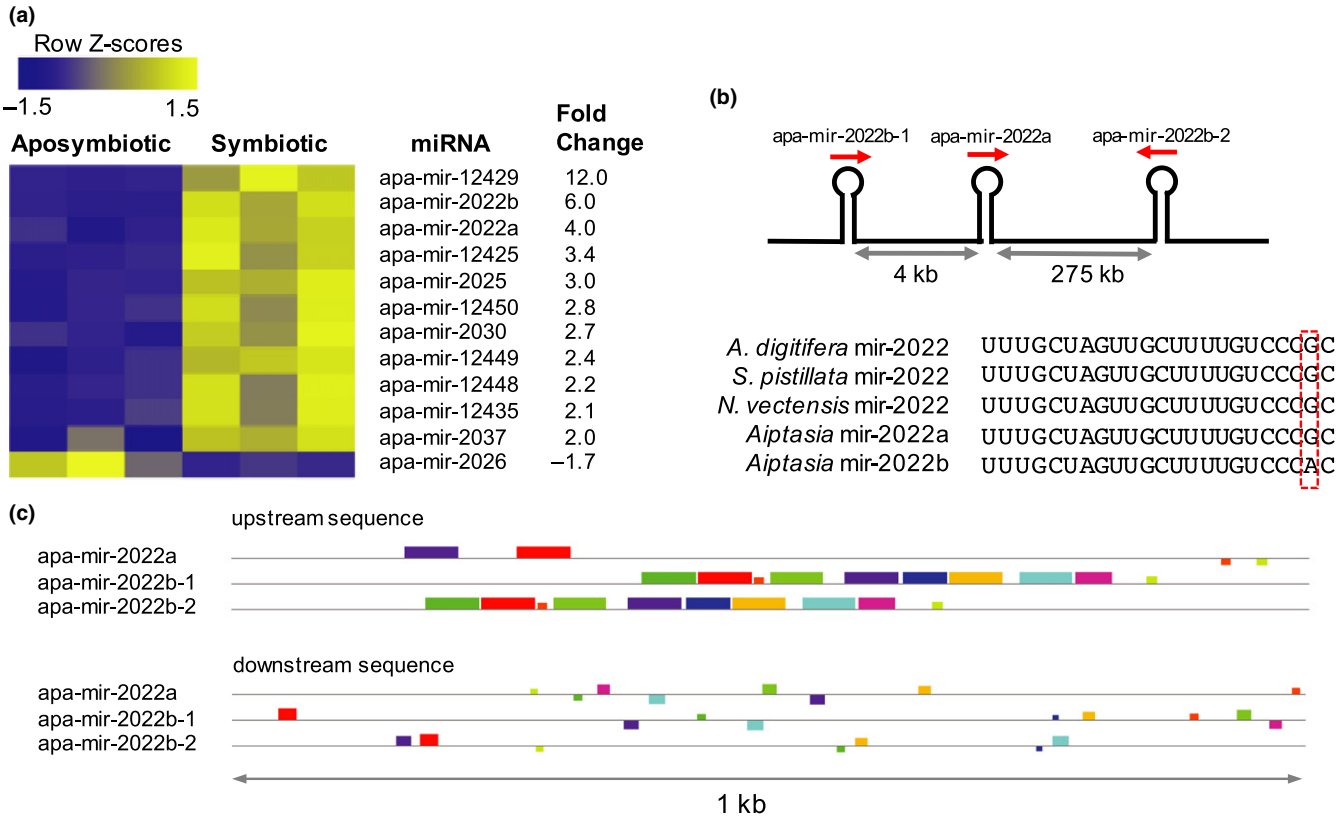


**FIGURE 4** Differential expression of miRNAs during establishment of the *Symbiodinium* endosymbiosis. (a) Heatmap of miRNAs with significant differential expression (FDR ≤ 0.01); most are upregulated in the symbiotic relative to the aposymbiotic state. The columns represent the six independent experiments (three with aposymbiotic animals and three with fully populated symbiotic animals). (b) Top, relative positions of the apa-mir-2022b and apa-mir-2022a loci in the *Aiptasia* genome. Grey arrows, distances in kilobases (kb) between the miRNA loci; red arrows, directions of transcription. Bottom, presence of apa-mir-2022a, but not apa-mir-2022b, also in other anthozoan genomes, the single nucleotide difference between the two miRNAs is highlighted in red. (c) Locations of conserved sequence motifs detected in the regions 1-kb upstream of the apa-mir-2022a and apa-mir-2022b loci (top) but not in the regions 1-kb downstream of the loci (bottom); in the downstream regions, only short fragments of the sequence motifs are present, and in seemingly random order. Each coloured box denotes a sequence motif that is conserved between two or among all three of the genomic loci (see Figure S3 for details of the actual sequences) [Colour figure can be viewed at wileyonlinelibrary.com]

In mammals, it has been shown that binding of as few as seven nucleotides in the 5′ seed region of a mature miRNA is sufficient for effective miRNA–mRNA binding (Bartel, 2009). In contrast, many of the interactions identified here seemed to include a much higher number of binding nucleotides from the miRNA, especially when directly compared to human CLIP data (Grosswendt et al., 2014; Kishore et al., 2011) (Figure 3f). While most human miRNA–mRNA interactions involve only eight miRNA nucleotides, nearly a third of the *Aiptasia* miRNA–mRNA interactions ($n$ = 1,061) have a complementarity to the mRNA target of ≥17 miRNA nucleotides (Figure 3f).

Such high complementarity has also been observed in other cnidarians (Moran et al., 2014) and may be related to regulation of the target mRNA by slicing, a mode of action like that of plant miRNAs and presumably an ancient mode of miRNA function (Moran et al., 2014). One interesting example of possible regulation involving such high complementarity is represented by the binding of apa-mir-12452 to the mRNA for a protein of the recently identified cnidarian Ficolin-like protein (CniFL) family, putative pattern-recognition receptors that appear to be present only in symbiotic anthozoans (Baumgarten et al., 2015) (Figure 3g).

## 3.3 | Regulation of *Aiptasia* miRNAs during the onset and maintenance of endosymbiosis

To investigate the possible role of miRNA-mediated post-transcriptional regulation in the onset and maintenance of cnidarian–dinoflagellate endosymbiosis, we analysed changes in miRNA expression using the small RNA libraries obtained from the three different stages of infection with *Symbiodinium* as described above. Overall, the *Aiptasia* miRNAs appeared to show substantial regulation by the symbiotic state, with 12 of the 46 annotated miRNAs having altered expression levels (FDR ≤0.01) between aposymbiotic and fully populated anemones (Figure 4a; Figure S2a). Interestingly, 11 of these 12, covering a wide range of absolute expression levels (Figure S2b), were upregulated in symbiotic anemones, and all but three of these 11 had already reached their maximal levels of upregulation at the intermediate time point of infection (Figure S2c). Interestingly, two of the most highly upregulated miRNAs, apa-mir-2022b and apa-mir-2022a, are encoded in one genomic region spanning 275 kb that includes two copies of the sequence for an apa-mir-2022b precursor transcript and one copy of the sequence for an apa-mir-2022a precursor transcript (Figure 4b, top). mir-2022 is widely conserved in anthozoans (Figure 2d), with a single locus encoding this miRNA found in the genomes of both *S. pistillata* and *N. vectensis* (Liew et al., 2014; Moran et al., 2014). The mature miRNA sequences of apa-mir-2022b and apa-mir-2022a differ in only one nucleotide position near the 3′ end (Figure 4b, bottom), which, together with the close genomic positions of the three loci, suggests a recent duplication of the apa-mir-2022a locus in the *Aiptasia* lineage.

To explore the possible coregulation of these three miRNAs, we searched for conserved sequence motifs in the 1-kb regions upstream of their loci. Interestingly, we found that the two apa-mir-2022b loci, separated by ~275 kb, share several long and highly conserved motifs in their upstream regions, whereas the upstream region of apa-mir-2022a is distinct (Figure 4c, top and Figure S3). The regions downstream of the three loci also show no comparable sequence conservation (Figure 4c, bottom). Because the exact transcription start sites of the primary (pri-) miRNA transcripts for the three loci are unknown, the motifs conserved between the two apa-mir-2022b loci could also lie within the pri-miRNA transcripts, so that the sequence conservation observed could be involved in cocontrol of either transcription or post-transcriptional processing of the pri-miRNA transcripts.

## 3.4 | Possible modulation of genes involved in symbiont acquisition and/or maintenance by *Aiptasia* miRNAs

Post-transcriptional control of gene expression by miRNAs usually results in the downregulation of cognate target genes either through endonucleolytic cleavage or inhibition of mRNA translation (Ghildiyal & Zamore, 2009). To assess possible changes of mRNA transcript levels due to the interactions with miRNAs, we measured mRNA levels in the same total RNA samples from the infection experiment that were used for the miRNA-expression and CLIP-tag analyses. In total, we found 885 interactions identified by CLIP between mRNA transcripts and the 12 miRNAs that showed significant differential expression, and thus are more likely to have a regulatory role in the endosymbiosis (see above).

For the 11 differentially expressed miRNAs that were upregulated in the symbiotic state (Figure 4a), we found interactions with a total of 289 putative target genes that also showed higher expression in the symbiotic state (log2 fold change > 0), 228 putative target genes that showed lower expression in the symbiotic state (log2 fold change < 0), and 108 putative target genes with no change in transcript abundance. For the single differentially expressed miRNA that was downregulated in the symbiotic state (apa-mir-2026), we found seven putative target genes that were upregulated and four that were downregulated, along with five putative target genes that did not show a measurable change in transcript abundance (Table S4). Thus, there was no general correlation in which changes in miRNA levels led consistently to inverse changes in the levels of the predicted target mRNAs.

However, upon closer examination of the putative target genes, we found several whose products have previously been implicated in the onset and/or maintenance of cnidarian–dinoflagellate endosymbiosis. These include a membrane receptor of the transforming growth factor β receptor family (TGFβR) (Detournay, Schnitzler, Poole, & Weis, 2012), in whose mRNA three sites were targeted by apa-mir-12450, apa-mir-12428, and apa-mir-2037, and the downstream messenger of TNF receptors, TRAF (Barshis et al., 2013), targeted at one site in its mRNA by apa-mir-12435. We also identified components of a putative fibroblast-growth-factor (FGF) signalling cascade including the extracellular ligand FGF (two sites, targeted by apa-mir-12424 and apa-mir-12448), its receptor (FGFR, five sites targeted by apa-mir-12449, apa-mir-12421, apa-mir-12438, apa-mir-

12441, apa-mir-2022a and apa-mir-2025), and a downstream intracellular messenger, GRB2 (one site, targeted by apa-mir-2022a and apa-mir-2022b), to be under possible post-transcriptional miRNA control. Although we saw no changes in levels of the TGFβR or GRB2 mRNAs, we found that the FGF, TRAF and FGFR mRNA decreased considerably in the symbiotic state, possibly reflecting the increases in the corresponding miRNAs (Table S4).

## 4 | DISCUSSION

The establishment and maintenance of cnidarian–dinoflagellate endosymbiosis is accompanied by marked changes in host gene expression (Baumgarten et al., 2015; Ganot et al., 2011; Lehnert et al., 2014; Rodriguez-Lanetty et al., 2006; Schnitzler & Weis, 2010; Voolstra et al., 2009). In this study, we identified the miRNAs of *Aiptasia* and analysed their expression patterns and mRNA targets in order to illuminate their possible roles in regulating these changes in gene expression. To do so, we first established high-throughput-sequencing cross-linking immunoprecipitation (HITS-CLIP) in *Aiptasia*. This protocol can be applied readily to any other cnidarian as well as any RNA-binding protein and its target mRNA transcripts of interest. Notably, the establishment of similar protocols in a variety of biological systems has helped to elucidate the crucial importance of RNA–protein interactions and mRNA homoeostasis in a variety of phenotypes (Änkö & Neugebauer, 2012; Licatalosi & Darnell, 2010) including specific interactions in cancer cells (van Kouwenhove, Kedde, & Agami, 2011), neurons (Darnell, 2013; Licatalosi et al., 2008; Ule et al., 2003) and endoparasite pathogenesis (Vembar, Macpherson, Sismeiro, Coppée, & Scherf, 2015). More broadly, we hope that the protocol described here will provide a foundation for further studies of RNA–protein interactions in basal metazoans in general and in particular in regard to their putative role in cnidarian–dinoflagellate endosymbiosis.

Our annotation of the *Aiptasia* miRNAs revealed a surprisingly low conservation of miRNA families within the cnidarian phylum compared to what is seen in bilaterians, consistent with observations on the other cnidarian species analysed to date (Moran et al., 2014). Even among the miRNAs that are conserved in sea anemones, we identified a species-specific difference, namely the duplications of the apa-mir-2022a locus, where both the altered sequence of the mature miRNA and the diverged upstream regions of the miRNA loci

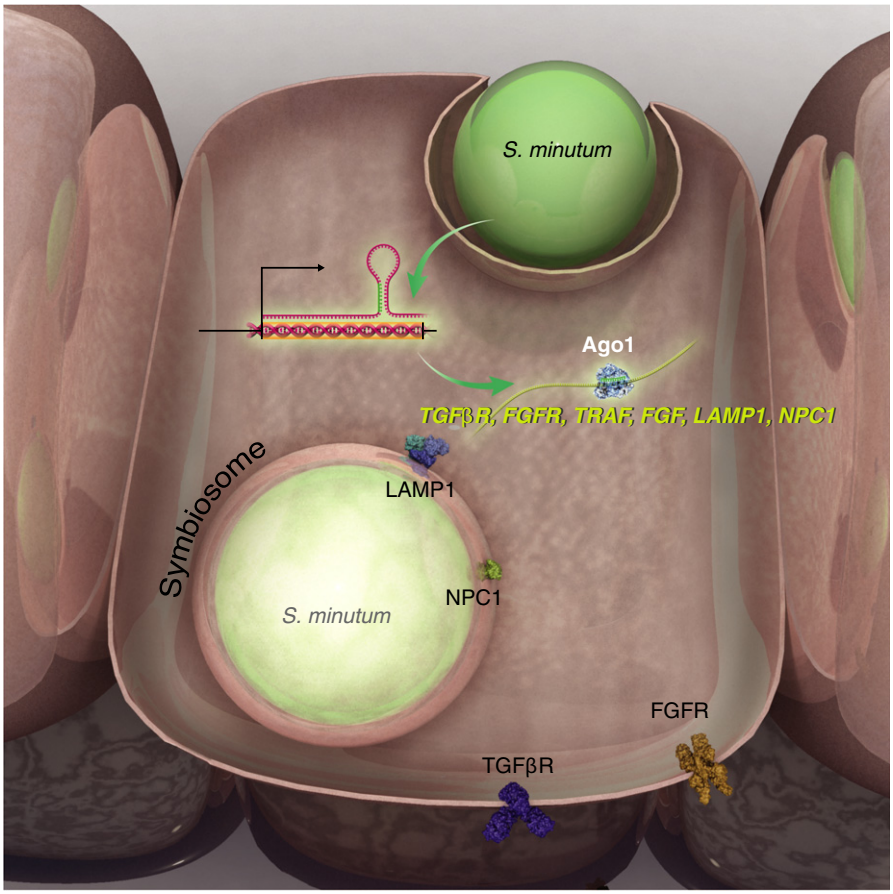


**FIGURE 5** Model of putative miRNA-mediated target gene modulation in endosymbiosis onset and/or maintenance. Diagram of an *Aiptasia* gastrodermal cell showing genes and pathways that are putatively regulated by differentially expressed miRNAs and function in biological processes previously hypothesized to be involved in endosymbiosis onset and/or maintenance [Colour figure can be viewed at wileyonlinelibrary.com]

indicate lineage-specific functional divergence. Moreover, the conservation of an individual nucleotide substitution in the 3′ region of the two apa-mir-2022b copies compared to apa-miR-2022a suggests a functional importance for nucleotide binding beyond the 5′ "seed" binding. This interpretation is consistent with the generally large hybridization length of the miRNA–mRNA duplex (i.e., the number of miRNA nucleotides involved in mRNA-target binding) observed in our CLIP data, in particular when compared to human miRNA–mRNA interactions. Similarly, miRNA-target studies in *N. vectensis* showed that besides miRNA-mediated translational repression (Mauri et al., 2017), cnidarian miRNAs might often lead also to target cleavage, presumably due to much higher complementarity between the miRNA and mRNA target transcript, as seen also in plant miRNAs (Moran et al., 2014).

Host gene expression is probably regulated by several mechanisms in response to *Symbiodinium* infection. In this context, the lack of a clear correlation between miRNA and target mRNA expression might point towards a miRNA-mediated, fine-scale modulation rather than a global regulation of gene expression. Furthermore, certain miRNA–mRNA interactions and the resulting putative modulation of target transcript levels might be restricted to a particular set of cells or tissues and so would not have been resolved in the current study. Even though the identified interactions cannot currently be functionally validated due to the absence of appropriate techniques to knock down or overexpress miRNAs in *Aiptasia*, the significant changes in miRNA expression do suggest that miRNA-mediated modulation of host gene expression constitutes one mechanism regulating the endosymbiotic relationship.

In particular, the identification of differentially expressed miRNAs that interact with mRNAs whose products are commonly considered to play key roles in endosymbiosis onset and/or maintenance can provide a model of how miRNA action may be involved in this process (Figure 5). For instance, the interaction of miRNAs with the mRNAs for FGFR, TGFβR and components of the TNFR/TRAF pathways (Figure 5) is particularly intriguing, as these proteins were previously suggested to be involved in the priming of immune and stress responses of symbiotic cnidarians, pathways that might have been co-opted during the evolution of mechanisms allowing a stable endosymbiosis (Barshis et al., 2013; Detournay et al., 2012). In addition, proteins that localize to the symbiosome membrane are thought to be critical for the establishment and/or maintenance of the endosymbiosis, including proteins involved in symbiosome maturation (Chen, Cheng, Hong, & Fang, 2004; Chen, Cheng, Sung, Kuo, & Fang, 2003) and in cross-membrane nutrient exchange (Dani, Ganot, Priouzeau, Furla, & Sabourault, 2014; Dani et al., 2017; Lehnert et al., 2014). In this context, we also identified miRNA-interacting mRNAs that encode proteins that are likely to be involved in the maintenance of the symbiosome, including a homolog of LAMP1, a protein related to lysosome—and potentially symbiosome—trafficking and maturation (Mohamed et al., 2016); a homolog of the sterol transporter NPC1 (Dani et al., 2014, 2017; Ganot et al., 2011; Lehnert et al., 2014); and a homolog of the peptide transporter ABCB9 (Davy et al., 2012). Of note, LAMP1 and NPC1 mRNA levels were reduced in symbiotic anemones, perhaps reflecting the binding of their regulatory miRNAs and arguing for a repressive effect in these particular cases (Table S4).

On a broader scale, recent studies on the interaction of plant roots and fungal pathogens have suggested that small RNAs (sRNAs) might also act in cross-kingdom RNA interference and regulation of gene expression (Weiberg, Wang, Bellinger, & Jin, 2014). Here, sRNAs of the fungal pathogen are expressed and translocated to the host cell and bound to plant Argonaute proteins to specifically downregulate host immunity genes (Weiberg et al., 2013). Even though we did not find previously identified *Symbiodinium* miRNAs or sRNAs that were bound to AipAgo1 in the experiments described here, a similar mechanism was recently hypothesized to function also in the coral–*Symbiodinium* endosymbiosis (Baumgarten et al., 2013; Lin et al., 2015).

Taken together, our data suggest that miRNAs are involved not only in defining the susceptibility of host organisms to endoparasites (Ghosh et al., 2013; LaMonte et al., 2012; Weiberg et al., 2014) but also in post-transcriptional modulations of gene expression that might be important in mutualistic relationships such as the dinoflagellate endosymbiosis in anemones and corals. With techniques now available such as the HITS-CLIP protocol described here, studies of this and other symbiotic systems must—and can—now also incorporate analyses of post-transcriptional levels of regulation.

## ACKNOWLEDGEMENTS

Research reported in this publication was supported by the King Abdullah University of Science and Technology (KAUST) and by Gordon and Betty Moore Foundation Grant 2629.01 (to J.R.P.). We thank the Bioscience Core laboratory and the Imaging and Characterization Core laboratory at KAUST for help with the protein characterization and microscopy. Figure 5 was created by Heno Hwang, scientific illustrator at KAUST.

## DATA ACCESSIBILITY

Small RNA sequences: NCBI SRA, Accession no. SRX1351928, SRX1351929, SRX1351930. mRNA sequences: NCBI SRA, Accession no. SRX757525, SRX757526, SRX757528. Sequences of mature miRNAs are deposited at miRBase at http://mirbase.org. CLIP sequences: NCBI SRA, Accession no. SRX1351926.

## CONFLICT OF INTERESTS

The authors declare no conflict of interests.

## AUTHOR CONTRIBUTIONS

S.B. and C.R.V. conceived and designed the research; S.B., M.J.C., L.T, C.T.M. and L.Y.E. performed the experiments. M.A. and J.R.P.

provided analytical tools; S.B. analysed the data; S.B., J.R.P. and C.R.V. wrote the manuscript.

## ORCID

*Manuel Aranda* http://orcid.org/0000-0001-6673-016X
*Christian R. Voolstra* http://orcid.org/0000-0003-4555-3795

## REFERENCES

Althammer, S., Gonzalez-Vallinas, J., Ballare, C., Beato, M., & Eyras, E. (2011). Pyicos: A versatile toolkit for the analysis of high-throughput sequencing data. *Bioinformatics*, *27*(24), 3333–3340. https://doi.org/10.1093/bioinformatics/btr570

Altschul, S. F., Gish, W., Miller, W., Myers, E. W., & Lipman, D. J. (1990). Basic local alignment search tool. *Journal of Molecular Biology*, *215*(3), 403–410. https://doi.org/10.1016/S0022-2836(05)80360-2

Änkö, M. L., & Neugebauer, K. M. (2012). RNA-protein interactions in vivo: Global gets specific. *Trends in Biochemical Sciences*, *37*, 255–262. https://doi.org/10.1016/j.tibs.2012.02.005

Bailey, T. L., Boden, M., Buske, F. A., Frith, M., Grant, C. E., Clementi, L., … Noble, W. S. (2009). MEME Suite: Tools for motif discovery and searching. *Nucleic Acids Research*, *37*(Suppl. 2), 202–208. https://doi.org/10.1093/nar/gkp335 https://doi.org/10.1093/nar/gkp335

Barshis, D. J., Ladner, J. T., Oliver, T. A., Seneca, F. O., Traylor-Knowles, N., & Palumbi, S. R. (2013). Genomic basis for coral resilience to climate change. *Proceedings of the National Academy of Sciences of the United States of America*, *110*(4), 1387–1392. https://doi.org/10.1073/pnas.1210224110

Bartel, D. P. (2009). MicroRNAs: Target recognition and regulatory functions. *Cell*, *136*(2), 215–233. https://doi.org/10.1016/j.cell.2009.01.002

Baumgarten, S., Bayer, T., Aranda, M., Liew, Y., Carr, A., Micklem, G., & Voolstra, C. (2013). Integrating microRNA and mRNA expression profiling in *Symbiodinium microadriaticum*, a dinoflagellate symbiont of reef-building corals. *BMC Genomics*, *14*(1), 704. http://www.biomedcentral.com/1471-2164/14/704 https://doi.org/10.1186/1471-2164-14-704

Baumgarten, S., Simakov, O., Esherick, L. Y., Liew, Y. J., Lehnert, E. M., Michell, C. T., … Voolstra, C. R. (2015). The genome of *Aiptasia*, a sea anemone model for coral symbiosis. *Proceedings of the National Academy of Sciences of the United States of America*, *112*, 11893–11898. https://doi.org/10.1073/pnas.1513318112 https://doi.org/10.1073/pnas.1513318112

Bolger, A. M., Lohse, M., & Usadel, B. (2014). Trimmomatic: A flexible trimmer for Illumina sequence data. *Bioinformatics*, *30*(15), 2114–2120. https://doi.org/10.1093/bioinformatics/btu170

Carthew, R. W., & Sontheimer, E. J. (2009). Origins and mechanisms of miRNAs and siRNAs. *Cell*, *136*(4), 642–655. https://doi.org/10.1016/j.cell.2009.01.035

Chen, M. C., Cheng, Y. M., Hong, M. C., & Fang, L. S. (2004). Molecular cloning of Rab5 (ApRab5) in *Aiptasia pulchella* and its retention in phagosomes harboring live zooxanthellae. *Biochemical and Biophysical Research Communications*, *324*(3), 1024–1033. https://doi.org/10.1016/j.bbrc.2004.09.151

Chen, M.-C., Cheng, Y.-M., Sung, P.-J., Kuo, C.-E., & Fang, L.-S. (2003). Molecular identification of Rab7 (ApRab7) in *Aiptasia pulchella* and its exclusion from phagosomes harboring zooxanthellae. *Biochemical and Biophysical Research Communications*, *308*(3), 586–595. https://doi.org/10.1016/s0006-291x(03)01428-1

Chi, S. W., Zang, J. B., Mele, A., & Darnell, R. B. (2009). Argonaute HITS-CLIP decodes microRNA-mRNA interaction maps. *Nature*, *460*(7254), 479–486. https://doi.org/10.1038/nature08170

Dani, V., Ganot, P., Priouzeau, F., Furla, P., & Sabourault, C. (2014). Are Niemann-Pick type C proteins key players in cnidarian-dinoflagellate endosymbioses? *Molecular Ecology*, *23*(18), 4527–4540. https://doi.org/10.1111/mec.12876

Dani, V., Priouzeau, F., Mertz, M., Mondin, M., Pagnotta, S., Lacas-Gervais, S., … Sabourault, C. (2017). Expression patterns of sterol transporters NPC1 and NPC2 in the cnidarian-dinoflagellate symbiosis. *Cellular Microbiology*, *19*, e12753. https://doi.org/10.1111/cmi.12753 https://doi.org/10.1111/cmi.12753

Darnell, R. B. (2013). RNA protein interaction in neurons. *Annual Review of Neuroscience*, *36*, 243–270. https://doi.org/10.1146/annurev-neuro-062912-114322

David, C. N. (1973). A quantitative method for maceration of hydra tissue. *Wilhelm Roux Archiv Für Entwicklungsmechanik Der Organismen*, *171*(4), 259–268. https://doi.org/10.1007/BF00577724

Davy, S. K., Allemand, D., & Weis, V. M. (2012). Cell biology of cnidarian-dinoflagellate symbiosis. *Microbiology and Molecular Biology Reviews: MMBR*, *76*(2), 229–261. https://doi.org/10.1128/MMBR.05014-11

Detournay, O., Schnitzler, C. E., Poole, A., & Weis, V. M. (2012). Regulation of cnidarian-dinoflagellate mutualisms: Evidence that activation of a host TGFbeta innate immune pathway promotes tolerance of the symbiont. *Developmental and Comparative Immunology*, *38*(4), 525–537. https://doi.org/10.1016/j.dci.2012.08.008

Dubinsky, Z., & Stambler, N. (2010). *Coral reefs: An ecosystem in transition*. New York, NY: Springer Science & Business Media.

Esau, C., Davis, S., Murray, S. F., Yu, X. X., Pandey, S. K., Pear, M., … Monia, B. P. (2006). miR-122 regulation of lipid metabolism revealed by in vivo antisense targeting. *Cell Metabolism*, *3*(2), 87–98. https://doi.org/10.1016/j.cmet.2006.01.005 https://doi.org/10.1016/j.cmet.2006.01.005

Friedlander, M. R., Chen, W., Adamidi, C., Maaskola, J., Einspanier, R., Knespel, S., & Rajewsky, N. (2008). Discovering microRNAs from deep sequencing data using miRDeep. *Nature Biotechnology*, *26*(4), 407–415. https://doi.org/10.1038/nbt1394

Friedlander, M. R., Mackowiak, S. D., Li, N., Chen, W., & Rajewsky, N. (2012). miRDeep2 accurately identifies known and hundreds of novel microRNA genes in seven animal clades. *Nucleic Acids Research*, *40*(1), 37–52. https://doi.org/10.1093/nar/gkr688

Ganot, P., Moya, A., Magnone, V., Allemand, D., Furla, P., & Sabourault, C. (2011). Adaptations to endosymbiosis in a cnidarian-dinoflagellate association: Differential gene expression and specific gene duplications. *PLoS Genetics*, *7*(7), e1002187. https://doi.org/10.1371/journal.pgen.1002187

Ghildiyal, M., & Zamore, P. D. (2009). Small silencing RNAs: An expanding universe. *Nature Reviews Genetics*, *10*(2), 94–108. https://doi.org/10.1038/nrg2504

Ghosh, J., Bose, M., Roy, S., & Bhattacharyya, S. N. (2013). *Leishmania donovani* targets Dicer1 to downregulate miR-122, lower serum cholesterol, and facilitate murine liver infection. *Cell Host & Microbe*, *13*(3), 277–288. https://doi.org/10.1016/j.chom.2013.02.005

Grimson, A., Srivastava, M., Fahey, B., Woodcroft, B. J., Chiang, H. R., King, N., … Bartel, D. P. (2008). Early origins and evolution of microRNAs and Piwi-interacting RNAs in animals. *Nature*, *455*(7217), 1193–1197. https://doi.org/10.1038/nature07415 https://doi.org/10.1038/nature07415

Grosswendt, S., Filipchyk, A., Manzano, M., Klironomos, F., Schilling, M., Herzog, M., … Rajewsky, N. (2014). Unambiguous identification of miRNA: Target site interactions by different types of ligation reactions. *Molecular Cell*, *54*(6), 1042–1054. https://doi.org/10.1016/j.molcel.2014.03.049 https://doi.org/10.1016/j.molcel.2014.03.049

Hambleton, E. A., Guse, A., & Pringle, J. R. (2014). Similar specificities of symbiont uptake by adults and larvae in an anemone model system for coral biology. *Journal of Experimental Biology*, *217*, 1613–1619. https://doi.org/10.1242/jeb.095679

Hofacker, I. L. (2003). Vienna RNA secondary structure server. *Nucleic Acids Research*, *31*(13), 3429–3431. https://doi.org/10.1093/nar/gkg599

Howe, E. A., Sinha, R., Schlauch, D., & Quackenbush, J. (2011). RNA-Seq analysis in MeV. *Bioinformatics*, *27*(22), 3209–3210. https://doi.org/10.1093/bioinformatics/btr490

Juliano, C. E., Reich, A., Liu, N., Gotzfried, J., Zhong, M., Uman, S., … Lin, H. (2014). PIWI proteins and PIWI-interacting RNAs function in *Hydra* somatic stem cells. *Proceedings of the National Academy of Sciences of the United States of America*, *111*(1), 337–342. https://doi.org/10.1073/pnas.1320965111 https://doi.org/10.1073/pnas.1320965111

Kishore, S., Jaskiewicz, L., Burger, L., Hausser, J., Khorshid, M., & Zavolan, M. (2011). A quantitative analysis of CLIP methods for identifying binding sites of RNA-binding proteins. *Nature Methods*, *8*(7), 559–564. https://doi.org/10.1038/nmeth.1608

van Kouwenhove, M., Kedde, M., & Agami, R. (2011). MicroRNA regulation by RNA-binding proteins and its implications for cancer. *Nature Reviews Cancer*, *11*(9), 644–656. https://doi.org/10.1038/nrc3107

Krishna, S., Nair, A., Cheedipudi, S., Poduval, D., Dhawan, J., Palakodeti, D., & Ghanekar, Y. (2013). Deep sequencing reveals unique small RNA repertoire that is regulated during head regeneration in *Hydra magnipapillata*. *Nucleic Acids Research*, *41*(1), 599–616. https://doi.org/10.1093/nar/gks1020

Krüger, J., & Rehmsmeier, M. (2006). RNAhybrid: MicroRNA target prediction easy, fast and flexible. *Nucleic Acids Research*, *34*(WEB. SERV. ISS.), 451–454. https://doi.org/10.1093/nar/gkl243 https://doi.org/10.1093/nar/gkl243

LaMonte, G., Philip, N., Reardon, J., Lacsina, J. R., Majoros, W., Chapman, L., … Chi, J. T. (2012). Translocation of sickle cell erythrocyte microRNAs into *Plasmodium falciparum* inhibits parasite translation and contributes to malaria resistance. *Cell Host & Microbe*, *12*(2), 187–199. https://doi.org/10.1016/j.chom.2012.06.007 https://doi.org/10.1016/j.chom.2012.06.007

Langmead, B., & Salzberg, S. L. (2012). Fast gapped-read alignment with Bowtie 2. *Nature Methods*, *9*(4), 357–359. https://doi.org/10.1038/nmeth.1923

Lehnert, E. M., Mouchka, M. E., Burriesci, M. S., Gallo, N. D., Schwarz, J. A., & Pringle, J. R. (2014). Extensive differences in gene expression between symbiotic and aposymbiotic cnidarians. *G3 (Bethesda)*, *4*(2), 277–295. https://doi.org/10.1534/g3.113.009084 https://doi.org/10.1534/g3.113.009084

Leung, A. K. L., & Sharp, P. A. (2013). Quantifying Argonaute proteins in and out of GW/P-bodies: Implications in microRNA activities. *Advances in Experimental Medicine and Biology*, *768*, 165–182. https://doi.org/10.1007/978-1-4614-5107-5_10

Licatalosi, D. D., & Darnell, R. B. (2010). RNA processing and its regulation: Global insights into biological networks. *Nature Reviews Genetics*, *11*(1), 75–87. https://doi.org/10.1038/nrg2673

Licatalosi, D. D., Mele, A., Fak, J. J., Ule, J., Kayikci, M., Chi, S. W., … Darnell, R. B. (2008). HITS-CLIP yields genome-wide insights into brain alternative RNA processing. *Nature*, *456*, 464–469. https://doi.org/10.1038/nature07488 https://doi.org/10.1038/nature07488

Liew, Y. J., Aranda, M., Carr, A., Baumgarten, S., Zoccola, D., Tambutté, S., … Voolstra, C. R. (2014). Identification of microRNAs in the coral *Stylophora pistillata*. *PLoS ONE*, *9*(3), e91101. https://doi.org/10.1371/journal.pone.0091101

Lin, S., Cheng, S., Song, B., Zhong, X., Lin, X., Li, W., … Morse, D. (2015). The *Symbiodinium kawagutii* genome illuminates dinoflagellate gene expression and coral symbiosis. *Science*, *350*(6261), 691–694. https://doi.org/10.1126/science.aad0408 https://doi.org/10.1126/science.aad0408

Mauri, M., Kirchner, M., Aharoni, R., Ciolli Mattioli, C., van den Bruck, D., Gutkovitch, N., … Chekulaeva, M. (2017). Conservation of miRNA-mediated silencing mechanisms across 600 million years of animal evolution. *Nucleic Acids Research*, *45*(2), 938–950. https://doi.org/10.1093/nar/gkw792 https://doi.org/10.1093/nar/gkw792

Mohamed, A. R., Cumbo, V., Harii, S., Shinzato, C., Chan, C. X., Ragan, M. A., … Miller, D. J. (2016). The transcriptomic response of the coral *Acropora digitifera* to a competent Symbiodinium strain: The symbiosome as an arrested early phagosome. *Molecular Ecology*, *25*(13), 3127–3141. https://doi.org/10.1111/mec.13659 https://doi.org/10.1111/mec.13659

Moore, M. J., Zhang, C., Gantman, E. C., Mele, A., Darnell, J. C., & Darnell, R. B. (2014). Mapping Argonaute and conventional RNA-binding protein interactions with RNA at single-nucleotide resolution using HITS-CLIP and CIMS analysis. *Nature Protocols*, *9*(2), 263–293. https://doi.org/10.1038/nprot.2014.012

Moran, Y., Fredman, D., Praher, D., Li, X. Z., Wee, L. M., Rentzsch, F., … Seitz, H. (2014). Cnidarian microRNAs frequently regulate targets by cleavage. *Genome Research*, *24*, 651–663. https://doi.org/10.1101/gr.162503.113 https://doi.org/10.1101/gr.162503.113

Moran, Y., Praher, D., Fredman, D., & Technau, U. (2013). The evolution of microRNA pathway protein components in Cnidaria. *Molecular Biology and Evolution*, *30*(12), 2541–2552. https://doi.org/10.1093/molbev/mst159

Muscatine, L., & Porter, J. W. (1977). Reef corals: Mutualistic symbioses adapted to nutrient-poor environments. *BioScience*, *27*(7), 454–460. https://doi.org/10.2307/1297526

Quinlan, A. R. (2014). BEDTools: The Swiss-army tool for genome feature analysis. *Current Protocols in Bioinformatics*, *47*, 11.12.1–11.12.34. https://doi.org/10.1002/0471250953.bi1112s47

R Development Core Team (2012). *R: A language and environment for statistical computing*. Vienna, Austria: R Foundation for Statistical Computing. Retrieved from http://www.r-project.org/

Robinson, M. D., McCarthy, D. J., & Smyth, G. K. (2010). edgeR: A bioconductor package for differential expression analysis of digital gene expression data. *Bioinformatics*, *26*(1), 139–140. https://doi.org/10.1093/bioinformatics/btp616

Rodriguez-Lanetty, M., Phillips, W. S., & Weis, V. M. (2006). Transcriptome analysis of a cnidarian-dinoflagellate mutualism reveals complex modulation of host gene expression. *BMC Genomics*, *7*, 23. https://doi.org/10.1186/1471-2164-7-23

Schnitzler, C. E., & Weis, V. M. (2010). Coral larvae exhibit few measurable transcriptional changes during the onset of coral-dinoflagellate endosymbiosis. *Marine Genomics*, *3*(2), 107–116. https://doi.org/10.1016/j.margen.2010.08.002

Shabalina, S. A., & Koonin, E. V. (2008). Origins and evolution of eukaryotic RNA interference. *Trends in Ecology & Evolution*, *23*(10), 578–587. https://doi.org/10.1016/j.tree.2008.06.005

Sunagawa, S., Wilson, E. C., Thaler, M., Smith, M. L., Caruso, C., Pringle, J. R., … Schwarz, J. A. (2009). Generation and analysis of transcriptomic resources for a model system on the rise: The sea anemone *Aiptasia pallida* and its dinoflagellate endosymbiont. *BMC Genomics*, *10*, 258. https://doi.org/10.1186/1471-2164-10-258 https://doi.org/10.1186/1471-2164-10-258

Tarver, J. E., Donoghue, P. C., & Peterson, K. J. (2012). Do miRNAs have a deep evolutionary history? *BioEssays: News and Reviews in Molecular, Cellular and Developmental Biology*, *34*(10), 857–866. https://doi.org/10.1002/bies.201200055

The RNAcentral Consortium (2015). RNAcentral: An international database of ncRNA sequences. *Nucleic Acids Research*, *43*, D123–D129. https://doi.org/10.1093/nar/gku991

Ule, J., Jensen, K. B., Ruggiu, M., Mele, A., Ule, A., & Darnell, R. B. (2003). CLIP identifies Nova-regulated RNA networks in the brain. *Science*, *302*(5648), 1212–1215. https://doi.org/10.1126/science.1090095

Vembar, S. S., Macpherson, C. R., Sismeiro, O., Coppée, J.-Y., & Scherf, A. (2015). The PfAlba1 RNA-binding protein is an important

regulator of translational timing in *Plasmodium falciparum* blood stages. *Genome Biology*, *16*(1), 212. https://doi.org/10.1186/s13059-015-0771-5

Voolstra, C. R., Schwarz, J. A., Schnetzer, J., Sunagawa, S., Desalvo, M. K., Szmant, A. M., … Medina, M. (2009). The host transcriptome remains unaltered during the establishment of coral-algal symbioses. *Molecular Ecology*, *18*(9), 1823–1833. https://doi.org/10.1111/j.1365-294x.2009.04167.x https://doi.org/10.1111/j.1365-294X.2009.04167.x

Weiberg, A., Wang, M., Bellinger, M., & Jin, H. (2014). Small RNAs: A new paradigm in plant-microbe interactions. *Annual Review of Phytopathology*, *52*(1), 495–516. https://doi.org/10.1146/annurev-phyto-102313-045933

Weiberg, A., Wang, M., Lin, F.-M., Zhao, H., Zhang, Z., Kaloshian, I., … Jin, H. (2013). Fungal small RNAs suppress plant immunity by hijacking host RNA interference pathways. *Science*, *342*(6154), 118–123. https://doi.org/10.1126/science.1239705 https://doi.org/10.1126/science.1239705

Weyn-Vanhentenryck, S. M., Mele, A., Yan, Q., Sun, S., Farny, N., Zhang, Z., … Zhang, C. (2014). HITS-CLIP and integrative modeling define the Rbfox splicing-regulatory network linked to brain development and autism. *Cell Reports*, *6*(6), 1139–1152. https://doi.org/10.1016/j.celrep.2014.02.005 https://doi.org/10.1016/j.celrep.2014.02.005

Xiang, T., Hambleton, E. A., DeNofrio, J. C., Pringle, J. R., & Grossman, A. R. (2013). Isolation of clonal axenic strains of the symbiotic dinoflagellate *Symbiodinium* and their growth and host specificity. *Journal of Phycology*, *49*(3), 447–458. https://doi.org/10.1111/jpy.12055

Yeo, G. W., Coufal, N. G., Liang, T. Y., Peng, G. E., Fu, X. D., & Gage, F. H. (2009). An RNA code for the FOX2 splicing regulator revealed by mapping RNA-protein interactions in stem cells. *Nature Structural & Molecular Biology*, *16*(2), 130–137. https://doi.org/10.1038/nsmb.1545

## SUPPORTING INFORMATION

Additional Supporting Information may be found online in the supporting information tab for this article.

**How to cite this article:** Baumgarten S, Cziesielski MJ, Thomas L, et al. Evidence for miRNA-mediated modulation of the host transcriptome in cnidarian–dinoflagellate symbiosis. *Mol Ecol*. 2018;27:403–418. https://doi.org/10.1111/mec.14452